Yeast Aim21/Tda2 both regulates free actin by reducing barbed end assembly and forms a complex with Cap1/Cap2 to balance actin assembly between patches and cables

Myungjoo Shin[a], Jolanda van Leeuwen[b], Charles Boone[b], and Anthony Bretscher[a,*]
[a]Department of Molecular Biology and Genetics, Weill Institute for Cell and Molecular Biology, Cornell University, Ithaca, NY 14853; [b]Donnelly Centre, University of Toronto, Toronto, ON M5S 3E1, Canada

ABSTRACT **How cells balance the incorporation of actin into diverse structures is poorly understood. In budding yeast, a single actin monomer pool is used to build both actin cables involved in polarized growth and actin cortical patches involved in endocytosis. Here we report how Aim21/Tda2 is recruited to the cortical region of actin patches, where it negatively regulates actin assembly to elevate the available actin monomer pool. Aim21 has four polyproline regions and is recruited by two SH3-containing patch proteins, Bbc1 and Abp1. The C-terminal region, which is required for its function, binds Tda2. Cell biological and biochemical data reveal that Aim21/Tda2 is a negative regulator of barbed end filamentous actin (F-actin) assembly, and this activity is necessary for efficient endocytosis and plays a pivotal role in balancing the distribution of actin between cables and patches. Aim21/Tda2 also forms a complex with the F-actin barbed end capping protein Cap1/Cap2, revealing an interplay between regulators and showing the complexity of regulation of barbed end assembly.**

Monitoring Editor
David G. Drubin
University of California, Berkeley

Received: Oct 12, 2017
Revised: Feb 13, 2018
Accepted: Feb 15, 2018

INTRODUCTION

The filamentous actin (F-actin) cytoskeleton provides eukaryotic cells with shape, contributes to surface structures, plays a role in cellular trafficking, and makes possible many motile and contractile events. A key question is how a cell can organize so many different actin-based functional structures at the same time, often drawing from the same subunit pool of free monomers, and regulate the balance between structures. The cell has many ways to do this, including localized F-actin assembly and disassembly and regulating the stability of F-actin-based structures. To address the role of actin in an experimentally accessible organism, we have been studying its function, assembly, and regulation in budding yeast.

Yeast has a single, essential gene encoding actin (Shortle *et al.*, 1982). During most of vegetative growth, two main actin-based structures are assembled: cortical patches and polarized cables (Adams and Pringle, 1984). Cortical patches are now known to be complex structures that provide the mechanical force for endocytosis (Kubler and Riezman, 1993; reviewed in Weinberg and Drubin, 2012; Goode *et al.*, 2015). The composition of cortical patches varies with time from their first appearance at sites of endocytosis to the propulsion of the endocytic vesicle into the cytoplasm (Kaksonen *et al.*, 2003, 2005). Cortical patch actin is nucleated by the Arp2/3 complex to generate a dendritic network, stimulated by several factors including Las17, Myo3, Myo5, Vrp1, Abp1, Bzz1, and Pan1 and modulated by the negative regulators Syp1, Lsb1, Lsb2, Sla1, Sla2, and Bbc1 (reviewed in Weinberg and Drubin, 2012; Goode *et al.*, 2015). Sla2 and Ent1 link the endocytic membrane to F-actin (Skruzny *et al.*, 2012). The assembly of actin at the barbed end is negatively regulated by capping protein Cap1/Cap2 and Abp1/Aim3 (Amatruda and Cooper, 1992; Kim *et al.*, 2004; Michelot *et al.*, 2013). Disassembly of actin filaments is mediated by cofilin (Cof1) and its cofactors, such as

This article was published online ahead of print in MBoC in Press (http://www.molbiolcell.org/cgi/doi/10.1091/mbc.E17-10-0592) on February 19, 2018.

The authors declare no competing financial interests.

Author contributions: J.v.L. and C.B. made the initial observations, M.S. and A.B. designed the experiments, M.S. performed the experiments, and M.S. and A.B. wrote and J.v.L. and C.B. edited the manuscript.

*Address correspondence to: Anthony Bretscher (apb5@cornell.edu).

Abbreviations used: CT, C-terminal region; F-actin, filamentous actin; G-actin, globular actin (monomeric actin); Lat-A, latrunculin-A; Lat-B, latrunculin-B; PP, polyproline; YPD, yeast extract peptone dextrose.

Aip1 (Adams and Pringle, 1984; Moon *et al.*, 1993; Carlier *et al.*, 1997; Ono *et al.*, 2004; Okada *et al.*, 2006). Although these are some of the key players, many other proteins also participate in the process (reviewed in Campellone and Welch, 2010; Goode *et al.*, 2015).

Actin cables are essential unbranched bundles of filaments extending from the bud and bud neck into the cytoplasm. They are nucleated and elongated by the formins: Bni1 localized to the bud cortex and Bnr1 at the bud neck (Fujiwara *et al.*, 1998; Kamei *et al.*, 1998; Evangelista *et al.*, 2002; Pruyne *et al.*, 2002; Sagot *et al.*, 2002a,b). They are stabilized by tropomyosin, Tpm1 and Tpm2, and their turnover is probably also mediated by cofilin, in conjunction with Aip1 (Liu and Bretscher, 1989a,b; Drees *et al.*, 1995; Okada *et al.*, 2006). Cables provide a track for the transport of organelles and mRNAs by the myosin-V motors, Myo2 and Myo4 (reviewed in Pruyne *et al.*, 2004). Myo2 is an essential protein, necessary for the transport of post-Golgi secretory vesicles for bud growth and the active inheritance of mitochondria (Johnston *et al.*, 1991; Pruyne *et al.*, 1998; Schott *et al.*, 1999; Chernyakov *et al.*, 2013). It also transports the vacuole, the Golgi, and peroxisomes to mediate their inheritance and orients the spindle in preparation for mitosis (Hill *et al.*, 1996; Catlett and Weisman, 1998; Yin *et al.*, 2000; Hoepfner *et al.*, 2001; Fagarasanu *et al.*, 2006; Lipatova *et al.*, 2008).

During growth, yeast has to balance the amount of actin devoted to cortical patches and cables. For example, cells lacking capping protein Cap1 or Cap2 have a low level of free actin due to excessive assembly of F-actin in cortical patches to the detriment of cables (Amatruda *et al.*, 1990, 1992). This is even more evident when an unregulated formin is expressed in yeast to generate excessive cables, which is lethal. This lethality can be suppressed by enhancing the assembly of actin in cortical patches (Gao and Bretscher, 2008).

Yeast can tolerate the loss of many actin-binding proteins. However, tropomyosin is essential as it stabilizes the filaments in cables. In its absence, cables are undetectable, resulting in depolarized growth and a failure to segregate organelles (Drees *et al.*, 1995; Pruyne *et al.*, 1998). Two genes encode tropomyosin, *TPM1* and *TPM2*. Tpm1 is about six times more abundant than Tpm2, so deletion of *TPM2* has little phenotype, whereas deletion of *TPM1* greatly slows growth (Liu and Bretscher, 1989a; Liu and Bretscher, 1992; Drees *et al.*, 1995). In *tpm1*Δ cells, F-actin nucleated by Bni1 and Bnr1 is stabilized by the very limiting amount of Tpm2, resulting in few and barely functional cables.

During genetic analysis, we found that the growth of *tpm1*Δ cells could be enhanced by deletion of Altered Inheritance of Mitochondria 21 (*AIM21*), a little-studied gene, implicated in mitochondrial inheritance and necessary for efficient endocytosis (Burston *et al.*, 2009; Hess *et al.*, 2009). We were surprised to find that *aim21*Δ cells have reduced numbers of actin cables, which presumably explains their defect in mitochondrial inheritance. Astonishingly, our initial studies revealed that loss of Aim21 partially restores cables to *tpm1*Δ cells. To resolve this apparent paradox, we set out to investigate the function of Aim21 and understand how its loss can restore cables to *tpm1*Δ cells.

While this article was being assembled, Farrell *et al.* (2017) reported the existence and characterization of the Aim21/Tda2 complex, its localization, and the structure of Tda2. We concur with much of their study and provide important new information about the mechanism of Aim21/Tda2 localization and uncover its function as a factor that regulates the assembly at the barbed end to balance the actin distribution between cables and patches.

RESULTS

Loss of the cortical patch protein Aim21 suppresses the growth defect of *tpm1*Δ cells

Cells lacking Tpm1 grow slowly due to a substantial reduction in the number of actin cables that support polarized growth (Liu and Bretscher, 1989a; Pruyne *et al.*, 1998). In a large-scale analysis of genetic suppressors, mutations in *AIM21* were identified as suppressors of the growth defect of *tpm1*Δ cells (personal communication in 2011, published in van Leeuwen *et al.*, 2016). This genetic suppression was recapitulated with freshly made deletion constructs showing that *tpm1*Δ cells grow slowly, *aim21*Δ cells grow at a rate similar to wild type (WT), and *aim21*Δ *tpm1*Δ cells have almost no growth defect (Figure 1A). Astonishingly, while *tpm1*Δ cells have almost no visible actin cables as seen using fluorescently labeled phalloidin and *aim21*Δ cells have reduced numbers, combining *aim21*Δ with *tpm1*Δ restores some cables to *tpm1*Δ cells (Figure 1, B and C). To understand this puzzling result, we first set out to determine the localization and function of Aim21. With this information in hand, we then addressed how *aim21*Δ can restore cables in *tpm1*Δ cells and suppress their growth defect.

To localize Aim21, we tagged the chromosomal gene with mNeonGreen. Live cell imaging showed Aim21-mNeonGreen was present in cortical punctate structures that colocalized with the actin patch marker Abp1-mCherry (Figure 1D). However, colocalization was not perfect. Since cortical patches are transient structures, we looked at these two proteins over time and found that Aim21-mNeonGreen and Abp1-mCherry appeared at the same time, but Aim21 left the patch ~1.5 s before Abp1-mCherry (Figure 1E). Abp1-mCherry assembles at cortical endocytic sites and then as the membrane undergoes scission to form an endocytic vesicle, it moves inward (Kaksonen *et al.*, 2003; reviewed in Weinberg and Drubin, 2012). Aim21-mNeonGreen colocalized with Abp1 up to the point where the inward movement initiated, suggesting that Aim21 leaves before, or soon after, endocytic scission and does not associate with endocytic vesicles (Figure 1E).

Much has been learned about actin assembly and dynamics by imaging the localization of cortical patch proteins in *sla2*Δ cells where the invagination of the endocytic membrane is uncoupled from actin assembly (Kaksonen *et al.*, 2003). As a result of this uncoupling, actin is continuously assembled adjacent to the plasma membrane and then moves inward as new actin subunits are added, thus providing a linear readout of this dynamic process. Imaging Aim21-mNeonGreen and Abp1-mCherry in *sla2*Δ cells revealed a tight localization of Aim21 close to the cell cortex, similarly to the localization seen for Sla1, Las17, and Pan1 and not with the older actin filaments in the Abp1-mCherry tail (Figure 1F) (Kaksonen *et al.*, 2003).

Aim21 is localized to cortical patches by Bbc1, Abp1, and Tda2

To determine how Aim21 is localized to cortical patches, we deleted each known cortical patch protein individually in cells with chromosomally tagged Aim21-GFP, but none completely eliminated cortical patch localization of Aim21-GFP. Therefore, we reasoned several proteins might contribute to Aim21 localization.

We first examined whether localization of Aim21 depended on F-actin. Cells treated with latrunculin to depolymerize all F-actin resulted in loss of much, but not all, cortical patch localization of Aim21-mNeonGreen (Figure 2A). Thus, there appears to be both actin-associated and actin-independent mechanisms of localization. Aim21 is a 679-residue protein with four polyproline regions (PP1–PP4) and an ~150 residue C-terminal (CT) domain (Figure 2B). All

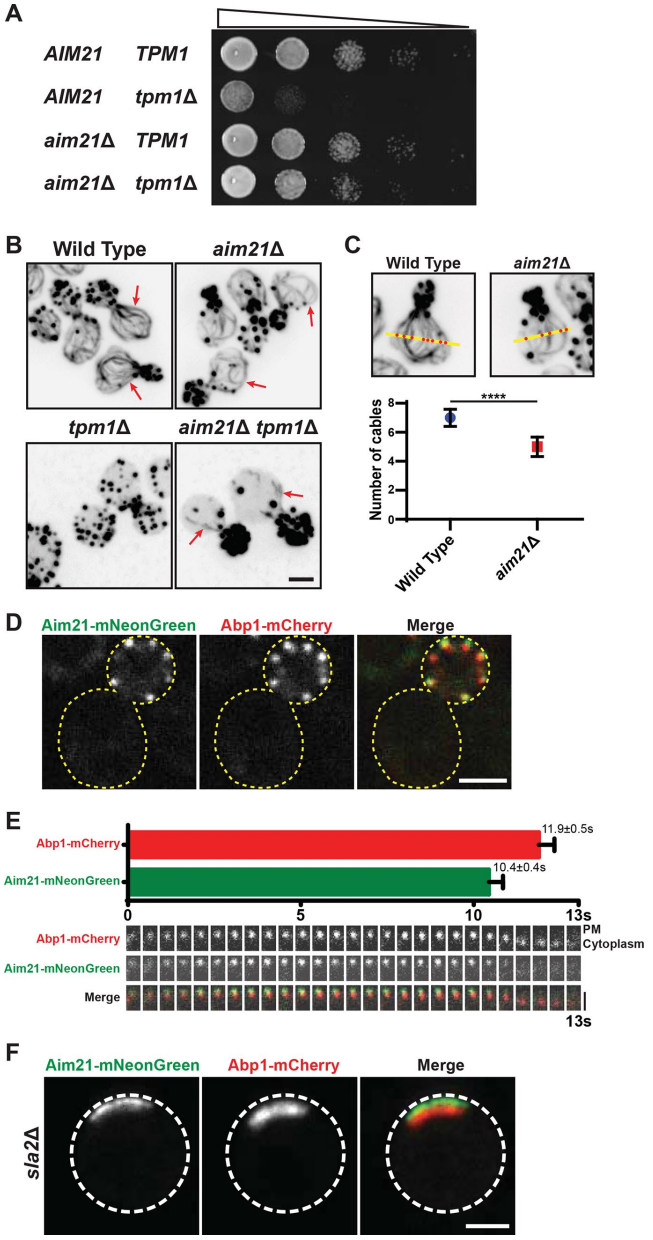

FIGURE 1: Deletion of actin patch protein Aim21 rescues the growth defect of *tpm1*Δ cells. (A) Serial dilution growth assay. Cells with the indicated genotypes were gown to $OD_{600} = 0.2$, subjected to 1:10 dilutions on a YPD plate, and incubated at 30°C for 1 d. (B) Actin structures as visualized by Alexa Fluor 568-phalloidin. Inverted images of maximum projection of whole cells. Red arrows indicate actin cables. Bar 2 µm. (C) The number of actin cables is reduced in *aim21*Δ cells compared with wild-type cells. A line was drawn at the center of the cell perpendicular to the mother–daughter axis. Red dots indicate intersections of this line and actin cables, which were used as a readout for the number of actin cables. Wild-type cells have 7.0 ± 0.3 (SEM) actin cables and *aim21*Δ cells have 5.0 ± 0.3 (SEM) actin cables ($n = 20$ for both). ****$p < 0.001$. Bars indicate 95% confidence intervals (CI). (D) Aim21-mNeonGreen colocalizes with Abp1-mCherry, an actin patch marker. Dotted lines outline the cells. Bar, 2 µm. (E) Bar graph and single-frame images of a cortical patch showing the duration of Abp1-mCherry and Aim21-mNeonGreen. On average, Aim21-mNeonGreen signal lasted 10.4 ± 0.4 (SEM) seconds and Abp1-mCherry signal lasted 11.9 ± 0.5 (SEM) seconds ($n = 13$). Bars indicate SEM. Scale bar, 1 µm. (F) Localization of Aim21-mNeonGreen and Abp1-mCherry in *sla2*Δ cells. Dotted lines outline the cells. Bar 2 µm.

four of these polyproline sequences are predicted to associate with SH3 domains, and it has been suggested that Aim21 binds the SH3 domains of Bbc1 and Abp1 (Fazi *et al.*, 2002; Tonikian *et al.*, 2009). We therefore generated GFP-tagged chromosomal constructs of Aim21 lacking various domains and assessed their localizations. We found that Aim21(PP4+CT) could not localize to patches (Supplemental Figure S1), suggesting that Aim21(PP1-3) is important for localization. Aim21(PP1-2) was the minimal region that could localize to cortical patches, and this localization was abolished in *bbc1*Δ cells (Figure 2C, top panel). Loss of Bbc1 also caused complete delocalization of Aim21 in latrunculin treated cells (Figure 2A). Thus, Bbc1 is necessary to localize this region of Aim21, most likely by direct interaction, and responsible for the actin-independent localization of Aim21, supported by the fact that the localization of Bbc1 is not dependent on actin (Supplemental Figure S2).

Aim21(PP1-4), lacking the CT domain, localized well to cortical patches in wild type and weakly in *bbc1*Δ cells; all localization was abolished in *bbc1*Δ *abp1*Δ cells (Figure 2C, middle panel). Thus, Aim21 requires Abp1 to enhance its localization through PP3-4. Interestingly, loss of Abp1 alone did not significantly decrease the localization of Aim21(PP1-4) to patches (Figure 2, C and D). Despite the involvement of Bbc1 and Abp1 in localizing Aim21, full-length Aim21-GFP still showed some localization in *bbc1*Δ *abp1*Δ cells, indicating some localization through the C-terminal domain (Figure 2C, bottom panel).

Tda2 is a small protein that high-throughput interaction data suggest interacts with Aim21 (Gavin *et al.*, 2006; Yu *et al.*, 2008). Because Tda2 does not have an SH3 domain, Tda2 was a likely candidate to interact with Aim21(CT). We therefore examined the localization of Aim21-GFP in *bbc1*Δ *abp1*Δ *tda2*Δ cells and found that it was no longer localized (Figure 2C, bottom panel). Overall, the data reveal that Aim21 has a complex interaction pattern, being localized by the two SH3-containing proteins Bbc1 and Abp1, with a contribution through the C-terminal domain involving Tda2 (quantified in Figure 2D and summarized in Figure 2E).

Having identified interactions involved in localization of Aim21, we examined how these interactions contribute to its distribution during actin assembly and turnover. We again used *sla2*Δ cells in which actin is assembled at the cortex and treadmills toward the cell center. In *sla2*Δ cells, Aim21-mNeonGreen is tightly associated with the cell cortex, whereas in *bbc1*Δ *sla2*Δ cells it is found throughout the tail (Figures 1F and 3, A and B). Thus, interaction of Aim21(PP1-2) with Bbc1, which itself is tightly associated with the cortex, restricts Aim21 to the cortex (Figure 3, A and B). As Bbc1 has an inhibitory function on actin assembly in patches through Las17, this phenotype could be due to the changed actin dynamics in *bbc1*Δ cells (Rodal *et al.*, 2003; Kaksonen *et al.*, 2005). To exclude this possibility, we examined the localization of Aim21(PP3-4+CT) in *BBC1 sla2*Δ cells. Loss of PP1-2 releases Aim21 from the cortex, and it is now found in the recently assembled two-thirds of the tail, very similar to the localization of capping protein Cap1 (Figure 3, A and B). Quantification of line scans along actin tails in *sla2*Δ cells supports the finding that Aim21-mNeonGreen is restricted to the cortex by Bbc1 and that interactions requiring Abp1 and Tda2 also play a role (Figure 3, C and D).

Aim21 regulates the abundance of actin in cortical patches and this regulation is necessary for efficient endocytosis

Phalloidin staining showed that the amount of F-actin in cortical patches is modestly enhanced in *aim21*Δ cells (Figure 4A). Using Abp1-mNeonGreen as a surrogate for quantifying cortical patch actin in living cells, patches in *aim21*Δ cells had significantly more

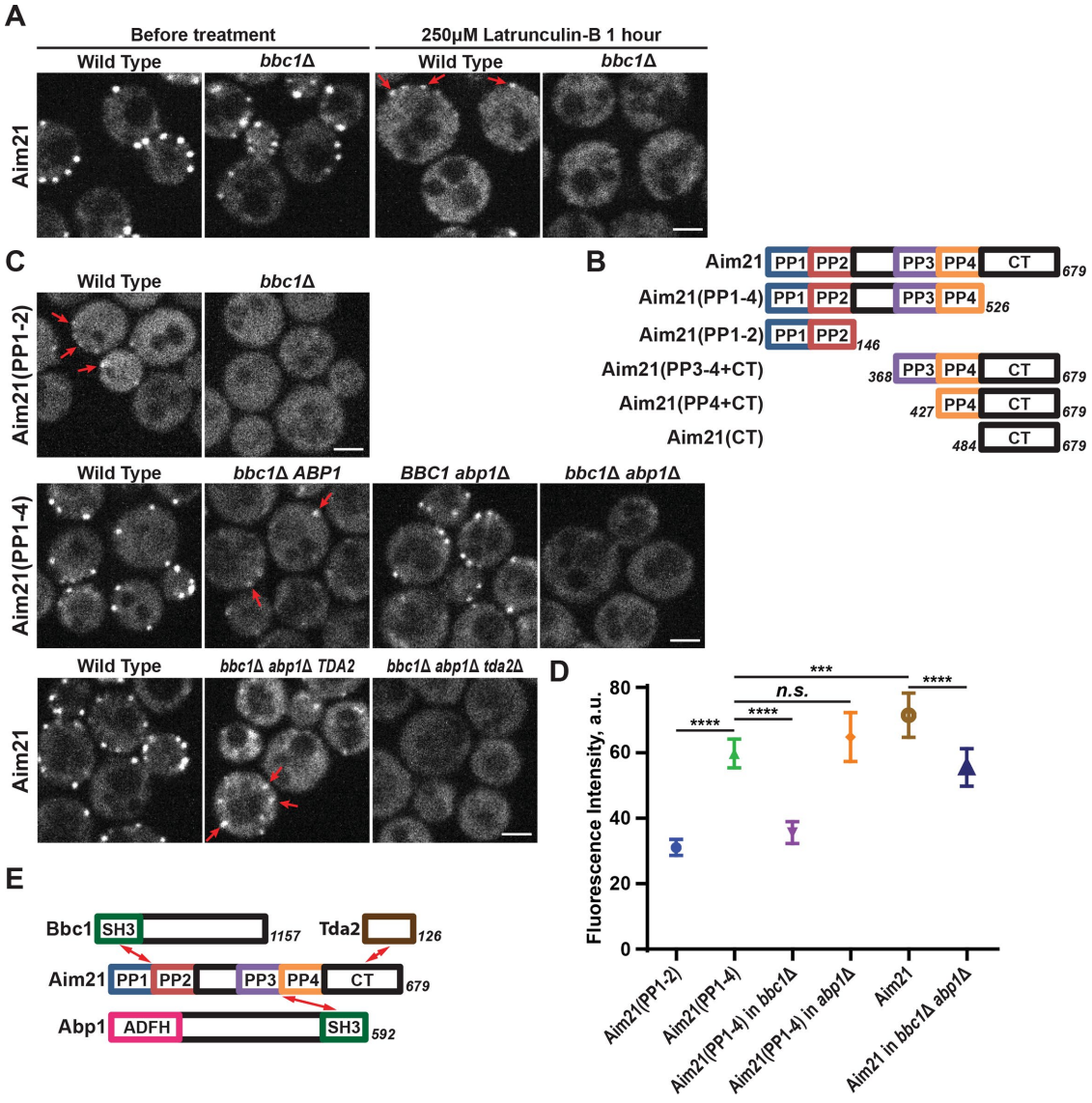

FIGURE 2: Localization of Aim21 to actin patches is dependent on Bbc1, Abp1, and Tda2. (A) Localization of Aim21-mNeonGreen before and after 1-h treatment with 250 μM latrunculin-B (Lat-B). Red arrows indicate localization to patches. (B) Schematic showing Aim21 protein structure and truncations used. Not to scale. (C) Aim21(PP1-2)-GFP, Aim21(PP1-4)-GFP, and Aim21-GFP in wild-type, *bbc1*Δ, *bbc1*Δ *abp1*Δ, and *bbc1*Δ *abp1*Δ *tda2*Δ cells. Red arrows indicate localization to patches. (D) Quantification of patch localization of Aim21 constructs. Arbitrary fluorescence unit (a.u.) was used to measure the fluorescence intensity. For Aim21(PP1-2), 31 ± 1 (SEM), $n = 29$; for Aim21(PP1-4), 60 ± 2 (SEM), $n = 50$; for Aim21(PP1-4) in *bbc1*Δ, 36 ± 2 (SEM), $n = 32$; for Aim21(PP1-4) in *abp1*Δ, 65 ± 4 (SEM), $n = 46$; for Aim21, 72 ± 3 (SEM), $n = 61$; and for Aim21 in *bbc1*Δ *abp1*Δ, 56 ± 3 (SEM), $n = 34$. Bars indicate 95% CI. ****$p < 0.0001$; ***$p < 0.001$; and *n.s.*, not significant. (E) Schematic showing the interactions that contribute to the localization of Aim21 to patches. Actin depolymerizing factor homology (ADFH), domain. (A, C) Bars, 2 μm.

Abp1 signal than in wild-type cells (Figure 4, B and C) and the lifespan of patches increased from ~11.9 s in wild type cells to 17.3 s in *aim21*Δ cells (Figure 4, D and E). These phenotypes are reminiscent of cells lacking capping protein Cap1 or Cap2, in which filaments in cortical patches overgrow, resulting in a reduced level of free actin available for assembly (Kaksonen *et al.*, 2005; Michelot *et al.*, 2013). We therefore wished to examine the level of free actin in *aim21*Δ cells compared with *cap1*Δ cells. The level of free actin can be indirectly assessed by testing the sensitivity of cells to growth inhibition by latrunculin—a low level of free actin renders the cells very sensitive to the drug. When a filter paper disk containing 5 μl of 0.2 mM latrunculin-A was placed on a thin lawn of wild-type, *aim21*Δ, or *cap1*Δ cells, the halo-shaped zone of growth inhibition of *aim21*Δ cells was larger than wild-type cells but smaller than *cap1*Δ cells, suggesting that loss of Aim21 reduces the pool of actin available for assembly (Figure 4, F and G). These results, combined with the reduction in cables seen in *aim21*Δ cells, implies that Aim21 influences the balance of actin between patches and cables at least in part by regulating the level of free actin for assembly.

Aim21 has been recovered in two high-throughput functional screens. The first, from which it derives its name (Altered Inheritance of Mitochondria 21), revealed a defect in mitochondrial inheritance, presumably because mitochondrial inheritance requires active transport along actin cables (Hess *et al.*, 2009). In the second, it was

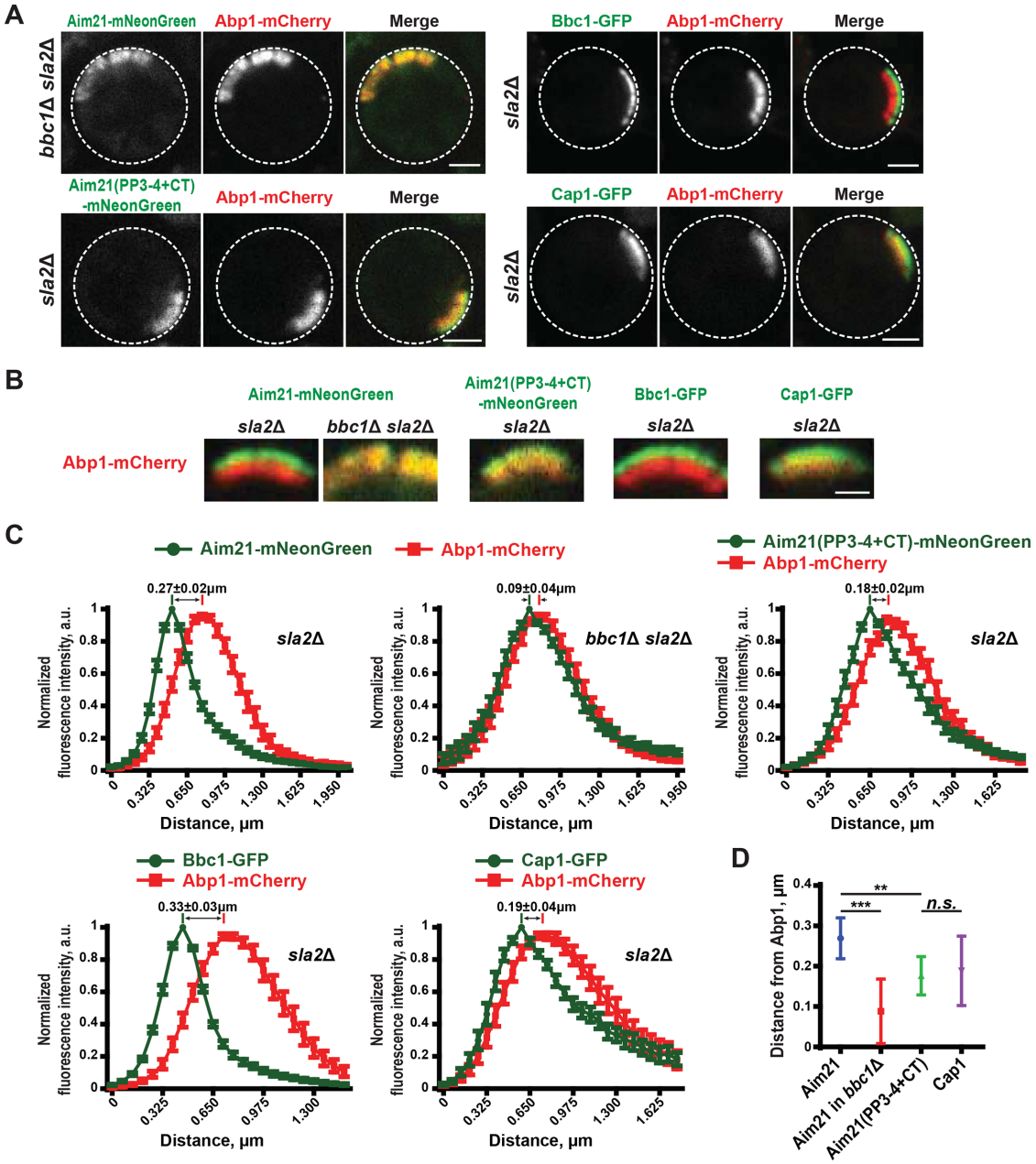

FIGURE 3: Interaction between Aim21(PP1-2) and Bbc1 is crucial for the cortical localization of Aim21. (A) Aim21-mNeonGreen in *bbc1*Δ *sla2*Δ, Bbc1-GFP in *sla2*Δ, Aim21(PP3-4+CT)-mNeonGreen in *sla2*Δ, and Cap1-GFP in *sla2*Δ. Abp1-mCherry as actin marker. Dotted lines outline the cells. Bar, 2 μm. (B) Magnified images of those shown in Figure 1F and A here. Bar, 2 μm. (C) Normalized localization of Aim21, Aim21(PP3-4+CT), Bbc1, and Cap1 with respect to Abp1 in *sla2*Δ or *bbc1*Δ *sla2*Δ. Intensity values of each color were normalized to the highest intensity, and the normalized values of both colors were aligned to the pixel with the highest green signal. For Aim21-mNeonGreen in *sla2*Δ, Aim21-mNeonGreen in *bbc1*Δ *sla2*Δ, and Aim21(PP3-4+CT)-mNeonGreen in *sla2*Δ, $n = 14$; for Cap1-GFP in *sla2*Δ, $n = 10$; and for Bbc1-GFP in *sla2*Δ, $n = 12$. Bars and ± indicate SEM. (D) Quantifications of the localizations in *sla2*Δ cells shown in C. Bars indicate 95% CI. ***$p < 0.001$; **$p < 0.01$; and *n.s.*, not significant.

recovered in a screen for genes affecting endocytosis of Snc1 (Burston *et al.*, 2009). A simple test of endocytosis is to test cells for their sensitivity to a toxic arginine analogue, canavanine. In the presence of arginine, wild-type cells down-regulate the arginine transporter, Can1, from the plasma membrane by endocytosis. Cells compromised for endocytosis cannot do this efficiently and, consequently, retain more transporters in the plasma membrane, which render the cells more sensitive to growth inhibition by canavanine. Consistent with earlier results, we find that *aim21*Δ cells are indeed more sensitive to canavanine, reflecting a partial defect in endocytosis (Figure 4H). Thus, the altered distribution of actin toward cortical patches influences their function, namely endocytosis.

The C-terminal region of Aim21 is required for its function, and this region interacts with Tda2

We next investigated which part of Aim21 is needed for its function. Since loss of Aim21 restores the growth of *tpm1*Δ cells, this rescue of growth inhibition provides an assay for Aim21 function. While

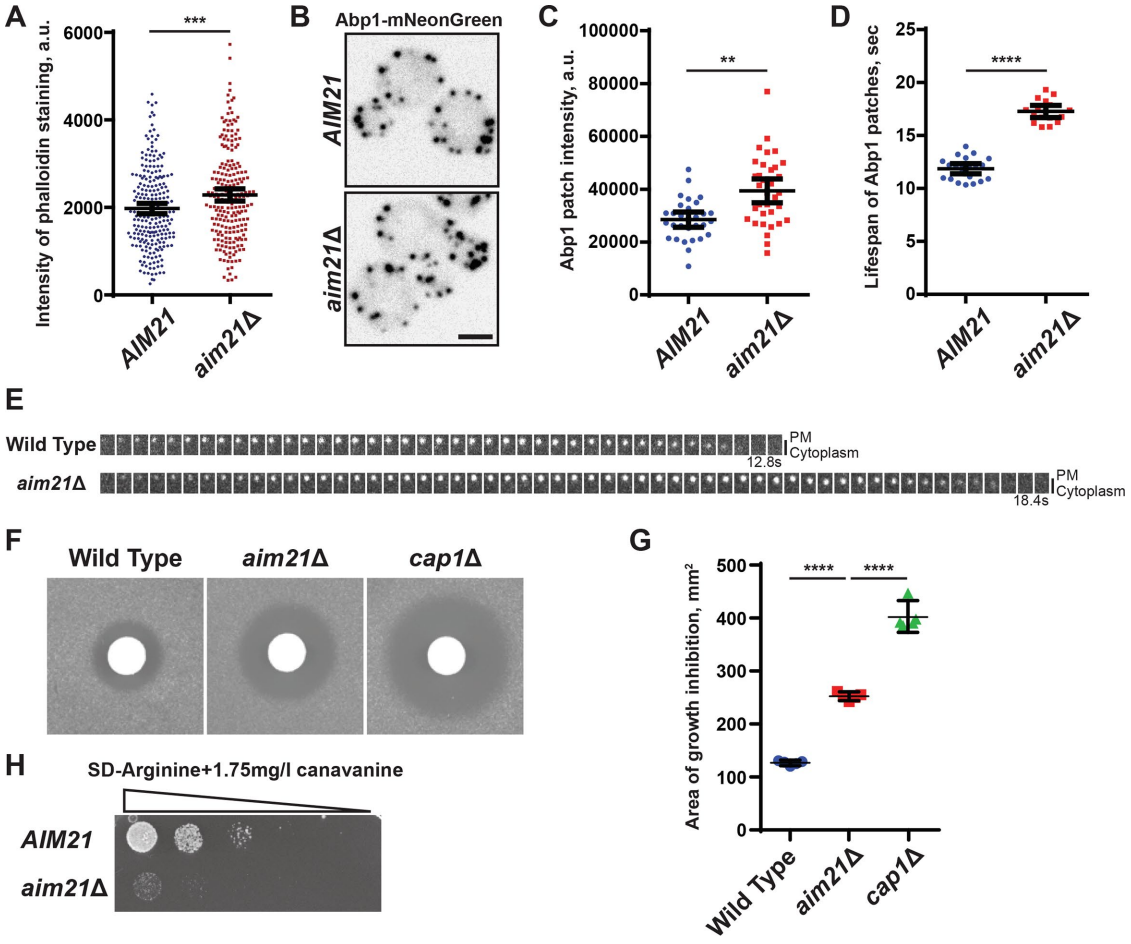

FIGURE 4: Aim21 inhibits actin assembly at actin patches. (A) Quantification of actin patch intensity in wild-type and *aim21*Δ cells. Actin structures were visualized by Alexa Fluor 568-phalloidin. Multiple planes, spanning the entire cell, were taken, and sum projection of the planes was used to calculate the amount of actin per patch. $n = 231$ for wild type and $n = 216$ for *aim21*Δ. ***$p < 0.001$. (B) Inverted images of Abp1-mNeonGreen in WT and *aim21*Δ cells. Bar, 2 μm. (C) Relative intensity of Abp1-mNeonGreen patches in WT and *aim21*Δ cells. $n = 30$ for WT and $n = 34$ for *aim21*Δ. **$p < 0.01$. (D) Lifespan of Abp1-mNeonGreen in patches. Middle five planes were taken and only patches that stayed in these five planes for their lifetime were included in the calculation. The average lifespan was 11.9 ± 0.23 (SEM) seconds ($n = 21$) for WT and 17.3 ± 0.27 (SEM) seconds ($n = 16$) for *aim21*Δ. ****$p < 0.0001$. (E) Single-frame images of Abp1-mNeonGreen patches in WT and *aim21*Δ cells. Bar, 1 μm. (F, G) Latrunculin sensitivity assay of WT, *aim21*Δ, and *cap1*Δ cells. Filter paper disks (6 mm) with 5 μl of 0.2 mM latrunculin-A (Lat-A) were used. The area of inhibited growth was measured and compared. The average area of inhibited was 127 ± 2 (SEM) mm^2 for wild type, 252 ± 3 (SEM) mm^2 for *aim21*Δ, and 403 ± 11 (SEM) mm^2 for *cap1*Δ ($n = 5$ for all). Bars indicate 95% CI. ****$p < 0.0001$. (H) Growth assay of the indicated cells spotted on synthetic arginine-deficient media plate with 1.75 mg/l of canavanine (SD-Arg+1.75 mg/l canavanine). (A, C, D, G) Bars indicate 95% CI.

AIM21 or *AIM21-GFP* cells in combination with *tpm1*Δ grew poorly, *tpm1*Δ *AIM21(PP1-4)-GFP* cells grew well, indicating that the C-terminal domain of Aim21 is necessary for function (Figure 5A). In vitro data with recombinant proteins shows that 6His-SUMO-Tda2 can pull down full-length Aim21 and Aim21(CT) but not Aim21(PP1-4) (Figure 5B). Thus, Tda2 binds directly to the C-terminal domain of Aim21. Consistent with these data, Tda2 localizes to cortical patches in wild-type cells but is delocalized in cells expressing chromosomal Aim21(PP1-4) and relocalized in *aim21*Δ cells in which the CT domain of Aim21 is fused to the cortical patch protein Bbc1 (Figure 5C and Supplemental S3). Thus, the interaction between Aim21(CT) and Tda2 not only contributes to the localization of Aim21 to patches (Figure 2, C–E) but also recruits Tda2 to patches.

As Aim21(CT) is important for the function of Aim21 and this region recruits Tda2, we explored if Tda2 contributes to Aim21 function. Indeed, *tda2*Δ can partially rescue the growth defect imposed by *tpm1*Δ (Figure 5D) and also reduces the level of free actin in cells as assayed by the latrunculin sensitivity assay (Figure 5, E and F). Neither the rescue of *tpm1*Δ nor the increase in latrunculin sensitivity by *tda2*Δ is as significant as seen for *aim21*Δ, indicating that Aim21 has additional functions to recruiting Tda2.

Aim21, Tda2, Cap1, and Cap2 form a complex

In addition to binding to Tda2, high-throughput screens suggest that Aim21 might interact with F-actin barbed end capping protein Cap1 and Cap2, which form an obligate heterodimer (Gavin *et al.*, 2006). To explore these relationships, we used in vitro assays to test possible interactions.

When resin-bound 6His-SUMO-Cap2 was incubated with Cap1, Aim21, and Tda2, all four proteins were recovered, indicating that

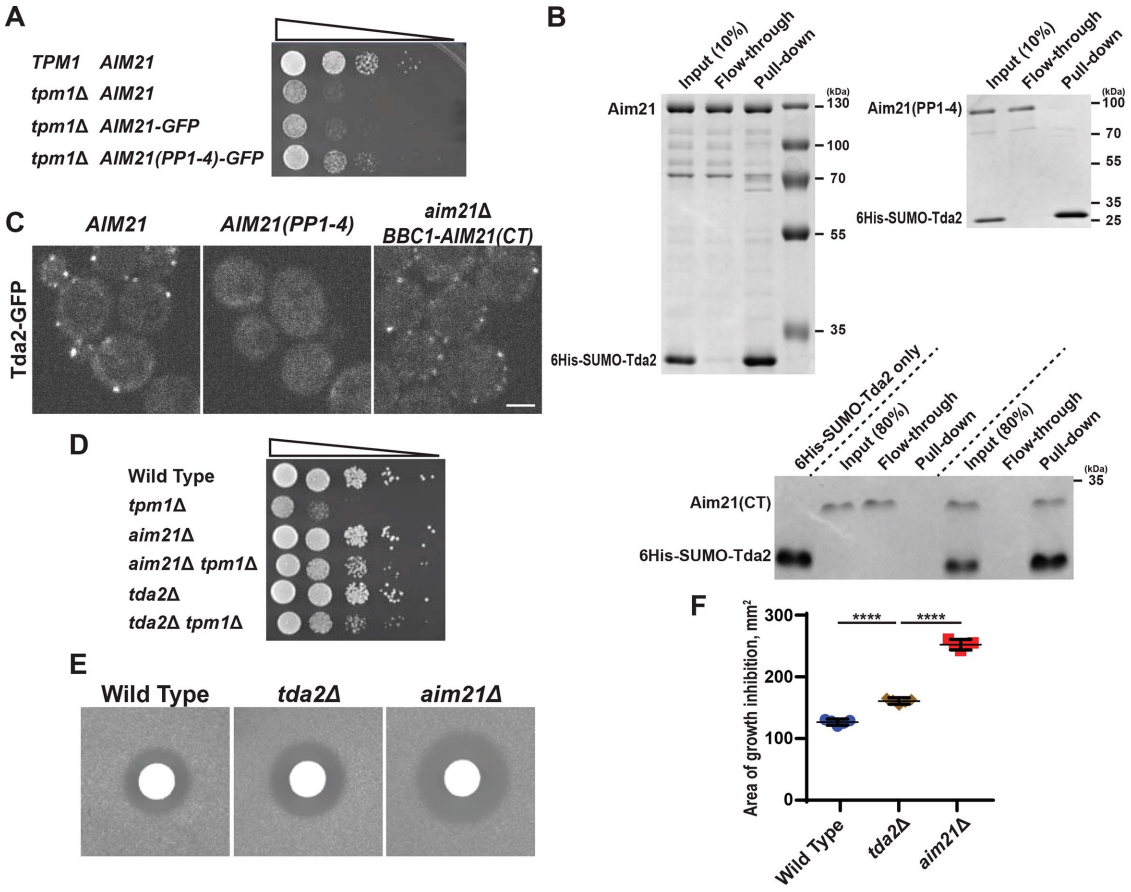

FIGURE 5: The C-terminal region (CT) of Aim21 is important for its cellular function and interacts with Tda2. (A) Serial dilution assay showing that *AIM21(PP1-4)-GFP* does not inhibit the growth of *tpm1*Δ cells as much as *AIM21*. YPD plate incubated at 30°C for 1 d. (B) Pull-down assay of Aim21, Aim21(PP1-4), or Aim21(CT) by 6His-SUMO-Tda2 using Ni-NTA resin. For Aim21 pull down and Aim21(PP1-4) pull down, Aim21 and Aim21(PP1-4) were used at 500 nM and 6His-SUMO-Tda2 was used at 1 μM. For Aim21(CT) pull down, Aim21(CT) was used at 340 nM, and 6His-SUMO-Tda2 were used at 1.2 μM. Aim21 forms a complex with Tda2 through Aim21(CT). Note: Aim21, Aim21(PP1-4), and Aim21(CT) all run higher than their calculated molecular weights (74.7, 57.6, and 21.7 kDa, respectively). Representative gel of $n \geq 3$ biological replicates shown. (C) Localization of Tda2-GFP in WT, *aim21*Δ, and *aim21*Δ *BBC1-AIM21(CT)*. Bar, 2 μm. (D) Serial dilution assay that shows *tda2*Δ partially rescues the growth defect of *tpm1*Δ cells. YPD plate incubated at 35.5°C for 1 d. (E, F) Latrunculin sensitivity assay of *tda2*Δ cells. Filter paper disks (6 mm) with 5 μl of 0.2 mM Lat-A were used. Images and data for wild type and *aim21*Δ are reproduced from Figure 4, F and G, for comparison. The average area of growth inhibition for *tda2*Δ was 161 ± 2 (SEM) mm^2 ($n = 5$). Bars indicate 95% CI. ****$p < 0.0001$.

Cap1/Cap2 binds to Aim21, Tda2, or the Aim21/Tda2 complex (Figure 6A, left panel). In a similar experiment, but employing Aim21(CT) in place of full-length Aim21, a complex of Cap1/Cap2/Tda2/Aim21(CT) formed (Figure 6A, right panel). The complex formed only when all components were present; without Aim21 or Tda2, the complex failed to form (Figure 6B).

We next explored whether loss of Aim21 or Tda2 had an effect on the localization of Cap1/Cap2. We found that Cap1-GFP remains localized to cortical patches and the amount of Cap1-GFP per patch in *aim21*Δ or *tda2*Δ cells does not significantly differ from that of wild-type cells (Figure 6, C and D). This was unexpected as actin cortical patches are larger and more persistent at least in *aim21*Δ cells (Figure 4, A–E). However, this is likely because most of Cap1/Cap2 complexes are already at the patches at any given time because of their high affinity to barbed ends. Thus, we conclude that Aim21 and Tda2 are not necessary to recruit Cap1/Cap2 to patches, and the effect Aim21/Tda2 has on patches seems to be largely independent of Cap1/Cap2 recruitment.

Aim21/Tda2 functions to reduce barbed end actin assembly

To explore the potential capping activities of these proteins, we utilized a pyrene-actin assembly assay; sheared filaments served actin nuclei, with a level of free actin so that most of elongation should occur at the barbed end of the growing filament. In this assay, assembly was dependent on the addition of the sheared filaments, with inclusion of 50 nM Cap1/Cap2 significantly inhibiting assembly (Figure 7A).

When we tested 50 nM Aim21/Tda2, it too reduced actin assembly, but not as efficiently as Cap1/Cap2 (Figure 7A). Tda2 alone had no effect on actin assembly, whereas Aim21 alone had a modest effect but much less than the Aim21/Tda2 complex (Figure 7A). These results explain why the level of free actin in *aim21*Δ cells, or *tda2*Δ cells, is lower than in wild-type cells. This finding then prompted us to examine whether Aim21/Tda2 complex binds to actin filaments. In cosedimentation assay, Aim21/Tda2 complex was enriched in actin filament pellets, suggesting that Aim21/Tda2 complex indeed binds to actin filaments to inhibit their elongation (Figure 7B).

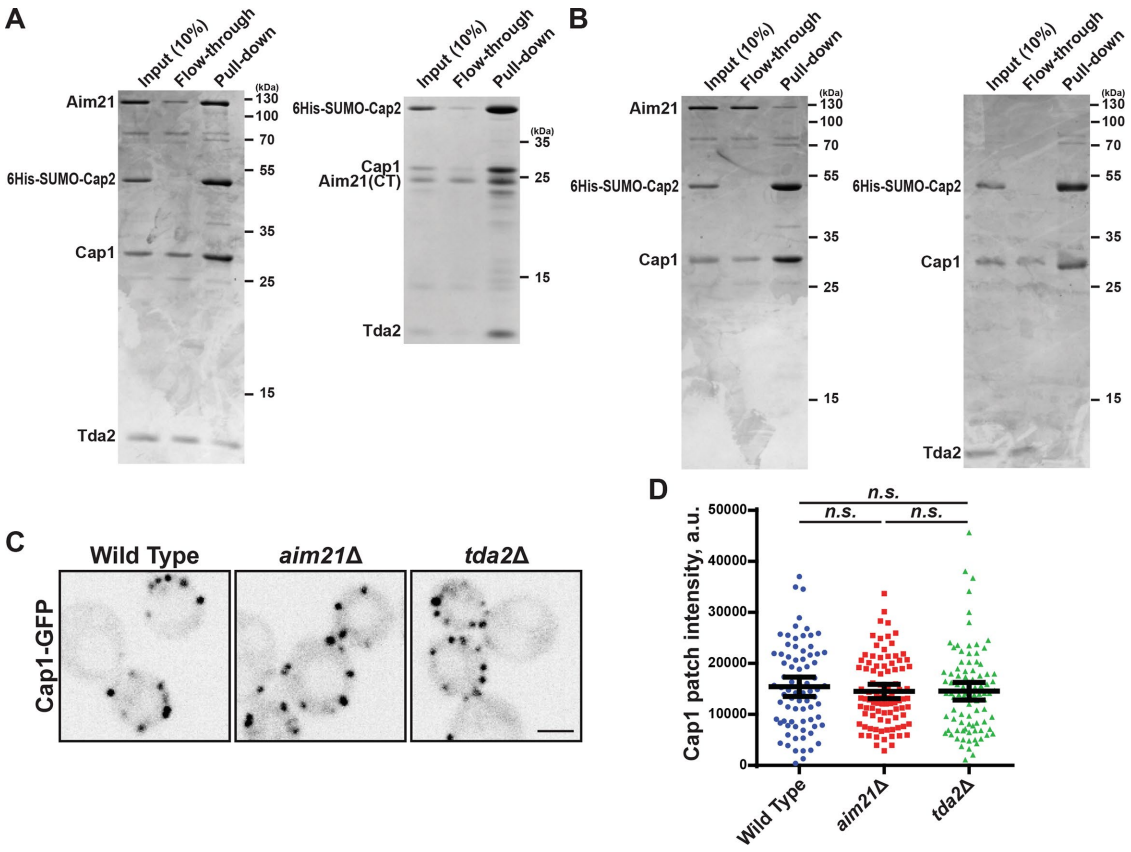

FIGURE 6: Aim21/Tda2 forms a complex with Cap1/Cap2. (A) Pull-down assay of Aim21 or Aim21(CT), Tda2, Cap1, and 6His-SUMO-Cap2, using Ni-NTA resin. Cap1/Cap2 forms a complex with Aim21/Tda2 or Aim21(CT)/Tda2. (B) Pull-down assay of Aim21, Cap1, and 6His-SUMO-Cap2; Tda2, Cap1, and 6His-SUMO-Cap2, using Ni-NTA resin. Cap1/Cap2 can only interact with Aim21 or Tda2 when both are present. (A, B) Aim21, Aim21(CT), Cap1, and 6His-SUMO-Cap2 were used at 1 μM. Tda2 was used at 2 μM. Representative gel of $n \geq 3$ biological replicates shown. (C) Inverted images of Cap1-GFP in WT, *aim21*Δ, and *tda2*Δ cells. Bar, 2 μm. (D) Brightness of Cap1-GFP patches in WT, *aim21*Δ, and *tda2*Δ cells. $n = 77$ for WT, $n = 91$ for *aim21*Δ, and $n = 91$ for *tda2*Δ. No statistically significant difference among them ($p > 0.4$). Bars indicate 95% CI. *n.s.*, not significant.

If Cap1/Cap2 and Aim21/Tda2 work at least partially independently to reduce barbed end assembly, then the effect of *aim21*Δ and *cap1*Δ should have an additive effect on actin structures in vivo. Indeed, *aim21*Δ *cap1*Δ cells show more depolarized actin structures, and their actin patches lasted longer than those of either *aim21*Δ or *cap1*Δ alone (Figure 7, C and D). Also, at 37°C, *aim21*Δ *cap1*Δ cells grow more slowly than either *aim21*Δ or *cap1*Δ alone (Figure 7E). Thus, Cap1/Cap2 and Aim21/Tda2 function, at least in part, independently.

*aim21*Δ favors actin assembly by Bnr1 to suppress the growth defect imposed by *tpm1*Δ

Our cell biological and biochemical data indicate that Aim21 functions to reduce assembly at the growing ends of filaments at patches to elevate the level of free actin available for assembly. If *aim21*Δ suppresses the growth defect of *tpm1*Δ cells by lowering the level of available actin, then we wondered if loss of other proteins that regulate free actin levels could also suppress *tpm1*Δ. Indeed, loss of capping protein Cap1, which reduces free actin levels (Figure 4, F and G), also partially suppressed the growth defect of *tpm1*Δ cells (Figure 8A). This suggests that lowering the level of free actin is a general mechanism for suppressing the growth defect of *tpm1*Δ cells. If correct, then *tpm1*Δ cells should grow better in a low level of latrunculin. Indeed, in a latrunculin sensitivity assay, *tpm1*Δ cells displayed a double halo; a region adjacent to the filter paper disk that inhibited growth by the high latrunculin level, surrounded by a region of better growth where the latrunculin level is reduced, with reduced growth on the periphery with too-low latrunculin levels (Figure 8B). Thus, *aim21*Δ restores growth to *tpm1*Δ cells by reducing the level of free actin for assembly.

As noted above, *aim21*Δ cells have fewer cables than wild-type cells, presumably because more actin is funneled into actin cortical patches (Figure 1C). So how can this suppress the growth defect of *tpm1*Δ cells? In yeast, tropomyosin is an essential protein as it is required to stabilize actin cables (Liu and Bretscher, 1989a,b; Pruyne *et al.*, 1998). Yeast has two tropomyosins, a major one, Tpm1, and a minor one, Tpm2, that is present at about one-sixth the level of Tpm1 (Drees *et al.*, 1995). Thus, in *tpm1*Δ cells, survival is dependent on the low level of Tpm2. Actin cables are nucleated and elongated by the two formins, Bni1 in the bud and Bnr1 at the bud neck. In *tpm1*Δ cells, both formins are active and generate actin cables, but they are very unstable due to the limiting supply of Tpm2.

Since polarized actin cables are essential for growth (Pruyne *et al.*, 1998), we quantitated the percentage of wild-type, *tpm1*Δ cells, and *aim21*Δ *tpm1*Δ cells that have cables (Figure 8E). In addition to confirming that *aim21*Δ *tpm1*Δ cells have more actin cables than *tpm1*Δ cells, a careful examination of the *aim21*Δ *tpm1*Δ cells indicated that the majority of cables emerged from the bud neck,

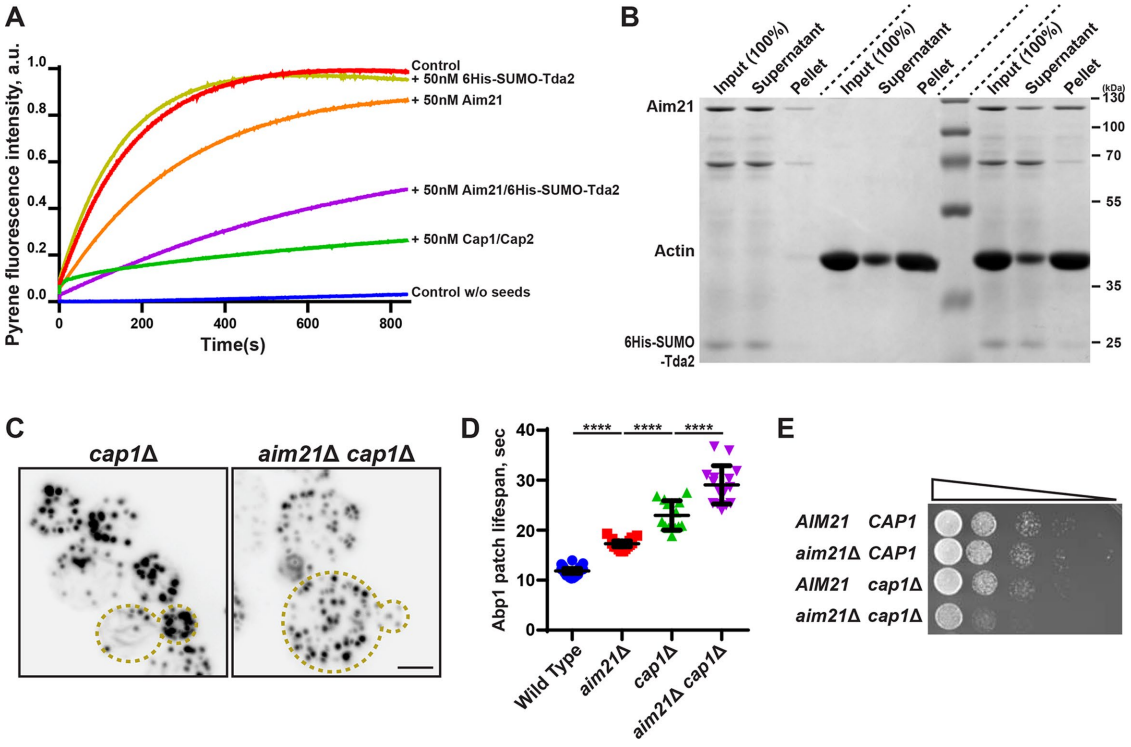

FIGURE 7: Aim21/Tda2 reduces assembly at the barbed end of actin filaments. (A) Pyrene actin assembly assays with 50 nM Cap1/Cap2, 50 nM Aim21, 50 nM 6His-SUMO-Tda2, or 50 nM Aim21/6His-SUMO-Tda2 using a final concentration of 1 µM actin. Both Cap1/Cap2 and Aim21/6His-SUMO-Tda2 significantly slow down the rate of actin assembly. Graph showing the average value of three independent experiments. Control w/o seeds contains G-actin and 10xF-actin buffer. Control contains G-actin, 10xF-actin buffer, and F-actin seeds. All additions were made at $t = 0$, and the assembly reaction was initiated by the addition of F-actin seeds. (B) Cosedimentation assay with actin filaments and Aim21/6His-SUMO-Tda2. F-actin (31 µM) was incubated with 600 nM Aim21/6His-SUMO-Tda2 at 4°C for 30 min. Actin filaments then got pelleted by centrifugation at 160,000 × *g* for 30 min at 4°C. Aim21 is enriched in the pellet fraction. Representative gel of $n \geq 3$ biological replicates shown. (C) Inverted images of actin structures in *cap1*Δ and *aim21*Δ *cap1*Δ cells, visualized by Alexa Fluor 568-phalloidin. Maximum projection of the entire cell. Dotted lines outline the cells. Bar, 2 µm. (D) Lifespan of Abp1 patches in wild type, *aim21*Δ, *cap1*Δ, and *aim21*Δ *cap1*Δ. Data points for wild type and *aim21*Δ are from Figure 4D and shown for comparison. The average lifespan was 23.0 ± 0.8 s (SEM) for *cap1*Δ (n = 13) and 29.1 ± 1.0 s (SEM) for *aim21*Δ *cap1*Δ (n = 15). Bars indicate 95% CI. ****$p < 0.0001$. (E) Serial dilution assay that shows that *aim21*Δ and *cap1*Δ have synthetic growth defect. YPD plate incubated at 37°C for 31 h.

the location of Bnr1. It has been found, at least in vitro, that the FH1-FH2-COOH region of Bnr1 is a much more potent nucleator than the equivalent region of Bni1 (Moseley and Goode, 2005). This immediately suggests a mechanism for suppression: whereas in *tpm1*Δ cells short ineffective cables are assembled by both Bni1 and Bnr1 (Figure 8F, second panel), in *aim21*Δ *tpm1*Δ cells cables are preferentially assembled from the bud neck by Bnr1. This allows the limiting Tpm2 to generate longer cables for more effective transport of secretory vesicles for polarized growth (Figure 8F, fourth panel). If this hypothesis is correct, then it should also be possible to suppress the growth defect of *tpm1*Δ cells by directing all cable assembly to Bnr1 by deleting *BNI1* (Figure 8F, fifth panel). Indeed, *bni1*Δ *tpm1*Δ cells grow better than *tpm1*Δ cells, and actin cables are restored, as in *aim21*Δ *tpm1*Δ (Figure 8, C–E).

DISCUSSION

Here we establish Aim21, with its cofactor Tda2, as a new complex that reduces barbed end assembly and whose activity in actin cortical patches is necessary for both efficient endocytosis and for regulating actin distribution between cables and cortical patches. Further, we elucidate how *aim21*Δ can partially rescue the loss of actin cables and the growth defect of *tpm1*Δ cells. While this study was in the final stages of assembly, a paper appeared describing the structure, localization, and potential function of Aim21/Tda2 (Farrell *et al.*, 2017). As indicated below, some of our results corroborate and extend this study and also importantly reveal the function of this protein complex.

Cells lacking Tpm1 are dependent on the minor tropomyosin isoform Tpm2 to stabilize actin cables, giving rise to few detectable cables and consequent slow growth (Liu and Bretscher, 1989a). Cells lacking Aim21 grow well, although they have a reduced number of cables. Our study originated from the paradox that *aim21*Δ *tpm1*Δ cells grow better and have more cables than *tpm1*Δ cells. Two lines of investigation initially pointed to a role for Aim21 in restricting actin assembly in cortical patches. First, Aim21 localized to cortical patches and loss of Aim21 enhanced the amount of actin in patches. Second, *aim21*Δ cells, like *cap1*Δ cells, were more sensitive to the monomer-sequestering drug latrunculin, indicating a low level of free actin available for assembly. By analyzing the localization and functionality of Aim21 truncations in vivo, we were able to identify the mechanism for cortical patch localization of Aim21, as well as the region required for its function. This revealed, in agreement with Farrell *et al.* (2017), that Bbc1 binding to the N-terminal polyproline regions (PP1-2) of Aim21 is a major determinant in the localization of Aim21. Consistent

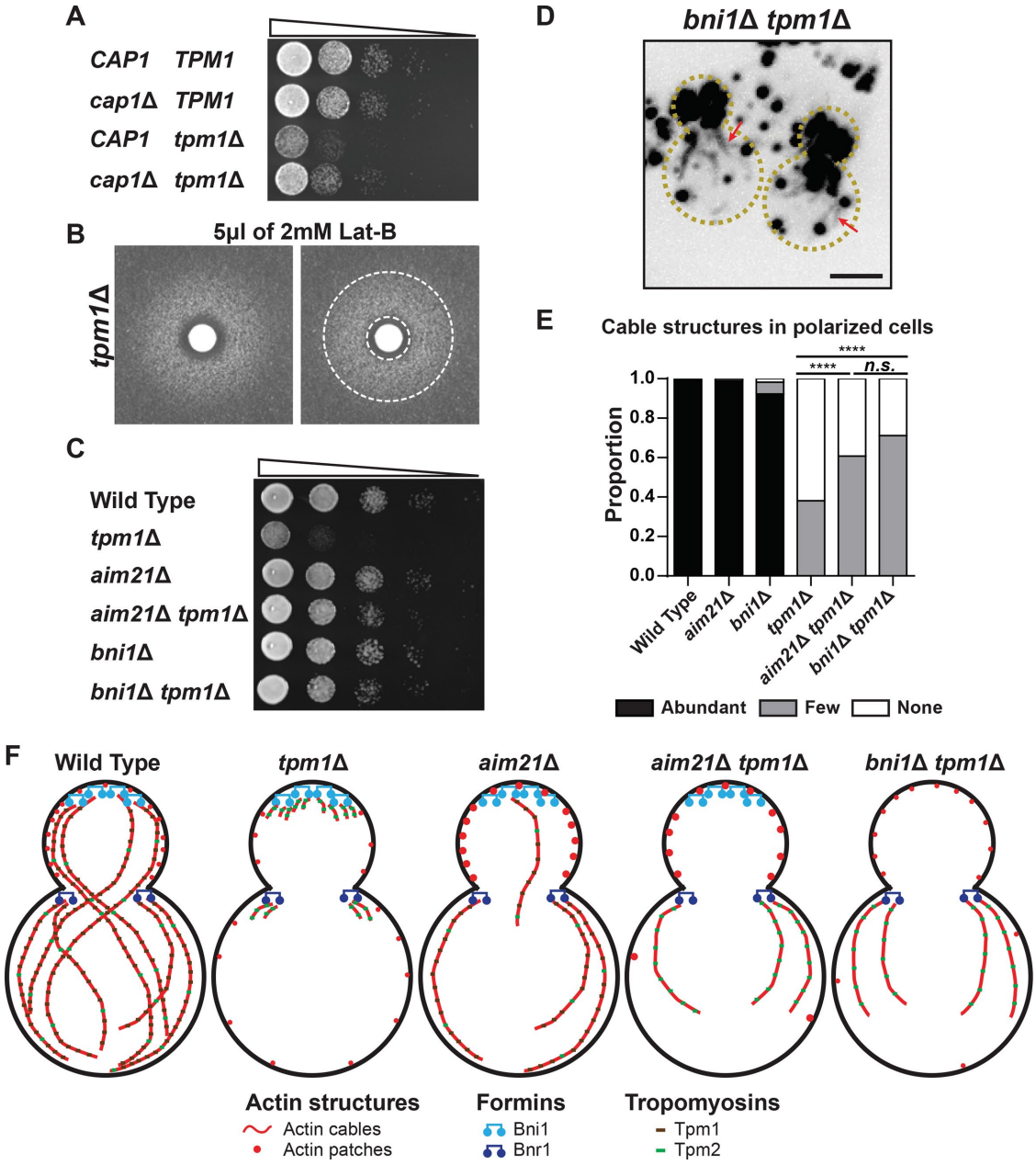

FIGURE 8: Decreasing the number of actin cables being initiated rescues the growth defect of *tpm1*Δ cells. (A) Serial dilution assay that shows *cap1*Δ partially rescues the growth defect of *tpm1*Δ cells. YPD plate incubated at 30°C for 1 d. (B) Latrunculin sensitivity assay on *tpm1*Δ cells. Filter paper disks (6 mm) with 5 µl of 2 mM Lat-B were used. The image on the right is the same as the one on the left but with dotted lines added to outline two halos. (C) Serial dilution assay that shows *bni1*Δ rescues the growth defect of *tpm1*Δ cells. YPD plate incubated at 35.5°C for 1 d. (D) Inverted image of actin structures in *bni1*Δ *tpm1*Δ cells, visualized by Alexa Fluor 568-phalloidin. Maximum projection of the entire cell. Dotted lines outline the cells. Red arrows indicate actin cables. (E) Quantification of actin cables in wild type, *tpm1*Δ, *aim21*Δ *tpm1*Δ, and *bni1*Δ *tpm1*Δ cells. Only cells with small- or medium-sized buds were included in the analysis. Abundant is defined as more than eight actin cables from the bud neck or bud tip. "Few" is defined as one to eight actin cables from the bud neck or bud tip. None is defined as no detectable actin cables. $n = 85$ for WT, $n = 189$ for *tpm1*Δ, $n = 125$ for *aim21*Δ *tpm1*Δ, and $n = 194$ for *bni1*Δ *tpm1*Δ. ****$p < 0.0001$. *n.s.*, not significant. (F) Model: *aim21*Δ rescues the growth defect of *tpm1*Δ cells by increasing the amount of actin in actin patches, thereby reducing G-actin availability in the cytoplasm and favoring the generation of fewer, but longer and stabilized actin cables nucleated by Bnr1. Supporting this model, *bni1*Δ also restores growth and cables to *tpm1*Δ cells.

with this, both Aim21 and Bbc1 are tightly associated with the cell cortex of the actin tail in *sla2*Δ cells, and Aim21 is redistributed throughout the tail when Bbc1 is deleted. Further, we identified an additional region, the third and fourth polyproline regions (PP3-4), as interacting with Abp1, and the C-terminal region, Aim21(CT), as necessary for its function and localization of Tda2 to cortical patches. The finding that a small amount of Aim21 still localizes to cortical patches in *bbc1*Δ *abp1*Δ cells and this is abolished by the additional

deletion of *TDA2* may reflect the ability of Tda2 to dimerize Aim21 and enhance otherwise weak interactions of the Aim21 monomer (Farrell *et al.*, 2017).

In vitro studies with purified proteins show that Tda2 physically binds to the C-terminal region of Aim21. Moreover, the Aim21/Tda2 complex can bind to Cap1/Cap2 in an interaction requiring Aim21(CT) and Tda2. Actin assembly assays reveal that Aim21 itself can reduce assembly of actin at the filament barbed end, whereas Tda2 cannot. Further, the Aim21/Tda2 complex is a better inhibitor but still less potent than Cap1/Cap2. Interestingly, addition of Aim21/Tda2 decreased the actin assembly inhibition by Cap1/Cap2 complex. This suggests that Aim21/Tda2 is not only an inhibitor in its own right but also a regulator of Cap1/Cap2. The formation of an Aim21/Tda2/Cap1/Cap2 complex is surprising given the different localizations of Aim21/Tda2 and Cap1/Cap2, an issue we return to below. Our data indicate that Cap1 abundance in cortical patches is independent of Aim21 or Tda2, suggesting that the conclusion of Farrell *et al.* (2017) that Aim21/Tda2 functions in the recruitment of Cap1/Cap2 may not be accurate.

F-actin in cortical patches is nucleated by the Arp2/3 complex, leaving barbed ends available for assembly. Elongation at barbed ends is regulated in part by the action of barbed end capping factors. The first and major factor identified was capping protein Cap1/Cap2, which form an obligate heterodimer, that has high affinity for barbed ends and prevents further addition of actin monomers to the barbed ends. However, in addition to Cap1/Cap2, other proteins also participate in inhibiting the elongation at barbed ends. Michelot *et al.* (2013) undertook a genetic screen to identify loss of function mutations that were more deleterious when combined with *cap1*Δ or *cap2*Δ. This approach identified two additional barbed end actin assembly inhibition complexes. First, Aip1 caps barbed ends in conjunction with the F-actin severing protein cofilin, Cof1. Second, Aim3 functions with Abp1 to inhibit actin assembly at barbed ends; all three are crucial for maintaining the free actin pool in cytoplasm. We now add Aim21/Tda2 as a fourth inhibitor for actin assembly. Although Aim21 and Tda2 did not come out of the genetic screen, it is interesting to note that *bbc1*Δ was found, potentially due to its role as a major recruiter necessary for the correct localization of Aim21/Tda2. Consistent with parallel roles for these actin assembly inhibitors, *aim21*Δ *cap1*Δ cells grow more slowly than *cap1*Δ cells. Interestingly, in *sla2*Δ cells where membrane invagination is uncoupled from actin assembly, the four different barbed end actin assembly inhibitors show very different and distinct localizations. Aim21/Tda2 is found with Bbc1 very close to the cell cortex, Cap1/Cap2 is found in the recently assembled region of the tail, Aip1 is found with cofilin on the older part of the tail, and Abp1/Aim3 is found throughout. This distinct localization, at least for Aim21, is necessary for full functionality; *AIM21(PP3-4+CT)* is only partially functional as it partially restores the growth defect to *aim21*Δ *tpm1*Δ cells (Supplemental Figure S4). Moreover, in *aip1*Δ cells, Cap1/Cap2 is found along the length of the whole tail, indicating competition between Cap1/Cap2 and Aip1 (Michelot *et al.*, 2013). In the absence of Aim21, the actin tails in *sla2*Δ cells were too short to confidently determine the localization of Cap1. However, in *bbc1*Δ cells, the restriction of Aim21/Tda2 to the cortex was lost and it is now found throughout the tail. Additionally, Aim21 and Aim3 both bind to Abp1 (Michelot *et al.*, 2013), presumably through the same SH3 domain, so the local environment likely influences where in the process they bind to Abp1. Layered on top of this, Ark1/Prk1 and Hrr25 kinases modulate endocytosis, and Aim21 is phosphorylated on multiple sites in vivo (Cope *et al.*, 1999; Albuquerque *et al.*, 2008; Peng *et al.*, 2015). These distinct localizations and regulation show that actin assembly at the barbed end is very carefully orchestrated, but the precise role of each of the four inhibitors will require further analysis.

Considering the distinct distributions of Aim21/Tda2 at the cortex and Cap1/Cap2 along the recently assembled part of the actin tail in *sla2*Δ cells, what is the significance of the Aim21/Tda2/Cap1/Cap2 complex? First, it should be noted that Cap1/Cap2 is estimated to be much more abundant than Aim21 or Tda2 (Kulak *et al.*, 2014), so a large percentage of the Cap1/Cap2 complex will not be associated with Aim21/Tda2. Second, this interaction might allow Aim21/Tda2 to remove Cap1/Cap2 from barbed ends. The association of Aim21/Tda2 with the region of actin assembly also suggests that one role is to reduce the activity of Cap1/Cap2 there, perhaps in conjunction with its known inhibition by the plasma membrane regulatory lipid $PI(4,5)P_2$ (Amatruda and Cooper, 1992).

The finding that Aim21 might regulate the amount of actin available for assembly did not initially explain how this restores growth to *tpm1*Δ cells or whether the lower level of available actin was related to the restoration of *tpm1*Δ cell growth. A number of subsequent observations indicated that reducing actin availability was indeed part of the mechanism of growth restoration. First, *tda2*Δ cells are also slightly more sensitive to latrunculin and *tda2*Δ also partially restores the growth of *tpm1*Δ cells. Second, *cap1*Δ cells are very sensitive to latrunculin because of their low levels of free actin and *cap1*Δ also partially restores growth to *tpm1*Δ cells. Third, whereas a high level of latrunculin inhibits the growth of *tpm1*Δ cells, an intermediate level can enhance their ability to grow. We traced the mechanism to the potency difference between formins, Bni1 and Bnr1 (Moseley and Goode, 2005). Our data indicate that lowering the level of free actin biases cable nucleation to Bnr1, thereby allowing the limiting supply of Tpm2 to stabilize longer cables from the bud neck. This enhances essential cable-dependent processes, such as the delivery of secretory vesicles and organelle segregation.

In summary, we have uncovered an additional mechanism for regulating actin assembly in budding yeast. Aim21 is conserved in yeast, including *Schizosaccharomyces pombe*, although not clearly present in other eukaryotes. Nevertheless, it raises the possibility that other organisms may have additional barbed end assembly inhibitors with specific localizations and functions.

MATERIALS AND METHODS

Yeast strains

Yeast transformations were performed according to Gietz and Schiestl (2007). Chromosomal manipulation used homologous recombination-based integration (Longtine *et al.*, 1998) and their genotypes were confirmed by PCR for correct integration. Yeast strains and plasmid constructs were used in this study are listed in Supplemental Tables S1 and S2, respectively.

To generate *AIM21(PP3-4+CT)* strains, chromosomal *AIM21* was deleted first and then replaced by *AIM21(PP3-4+CT)-GFP* or *AIM21(PP3-4+CT)-mNeonGreen*. To generate the *aim21*Δ *BBC1-AIM21(CT)* strain, we first made the *AIM21-mCherry* strain and then, from its genomic DNA, amplified the *AIM21(CT)-mCherry* region including the selectable marker with flanking sequences that target the C-terminus of *BBC1* by PCR. This PCR product was transformed into *aim21*Δ to make *aim21*Δ *BBC1-AIM21(CT)-mCherry*.

Microscopy and analysis

Images were acquired using a spinning disk confocal microscope (Intelligent Imaging Innovations, Denver, CO). It consisted of an inverted microscope (Leica DMI6000B), a spinning disk confocal unit (Yokogawa CSU-X1), a fiber-optic laser light source, a 100× 1.47NA field planarity (PL) apochromat (APO) objective lens, and a scientific

Complementary Metal–Oxide–Semiconductor (sCMOS) camera (Hamamatsu ORCA Flash 4.0v2+). SlideBook 6.0 software was used to operate the microscope system and analyze the images. Multiplane images were taken at 0.28-μm steps, and maximum or sum intensity projections were created with SlideBook software.

Cells grown at room temperature to their log phase were used for imaging both for live cell imaging and phalloidin staining. All imaging was done at 26°C. Cells were immobilized on concanavalin A–coated glass bottom culture dishes (MatTek) and supplemented with synthetic complete media or on 1.5% agarose gel beds made with synthetic complete media. Visualization of F-actin in yeast cells using fluorophore-conjugated phalloidin was done as described by Pringle *et al*. (1989), with a few modifications. We used 4% of paraformaldehyde to fix the cells and 3% (vol/vol) Alexa Fluor 568 phalloidin (Thermo Fisher Scientific A12380) in phosphate-buffered saline. Differential interference contrast (DIC) images were taken together with fluorescence images and used to outline the cells when they cannot be clearly defined from fluorescence images alone.

For analysis of the number of actin cables, a line was drawn perpendicular to the mother–daughter axis at the center of the mother cell and the number of intersections of this line and actin cables was counted. For analysis of Aim21 localization, the GFP signal intensities of different Aim21 constructs at patches were measured, and the background was set by selecting the same sized area outside of the cell because of the different cytoplasmic levels of Aim21 constructs. For analysis of actin patch intensity, Abp1 patch intensity, and Cap1 patch intensity, the background was set by selecting the same sized area inside the cell next to the patches that were selected for analysis. For analysis of Abp1 patch lifespan, center 5 planes (0.28-μm distance between planes) were taken and only the patches that disappeared in the center three planes were included for analysis to exclude the patches that simply moved out of the capture area. For analysis of localizations in *sla2*Δ cells, green and red intensities were measured along a line perpendicular to the plasma membrane. Intensities values were aligned to the pixel with the highest green signal.

For statistical analysis, Student's *t* test was used to determine *p* values.

Latrunculin sensitivity assay

Latrunculin sensitivity assay was done as described by Winder *et al*. (2003). Yeast cells were grown to log phase in synthetic complete media and 40 μl of the cultures were diluted into 2 ml of 2xYPD. The amount of 2 ml of 1% molten agarose cooled down to 55°–60°C was added. The mixture was briefly vortexed and poured on a yeast extract peptone dextrose (YPD) plate evenly. The plates were then incubated for 3 h at room temperature for the agarose to solidify and for yeast cells to recover from potential heat shock. Sterile 6-mm filter paper disks that absorbed 5 μl of 0.2 mM latrunculin-A (Lat-A) or 2 mM latrunculin-B (Lat-B) were then placed on top of the cells embedded in the agarose gel. The plates were incubated at 27°C for 24–48 h. For statistical analysis, Student's *t* test was used to determine *p* values.

Protein purification

pE-SUMOpro from LifeSensors was used to create plasmids that express 6His-SUMO-Aim21, 6His-SUMO-Aim21(PP1-4), 6His-SUMO-Aim21(CT), 6His-SUMO-Cap1, 6His-SUMO-Cap2, and 6His-SUMO-Tda2. These plasmids were transformed into Rosetta 2 (DE3) pLysS cells from Novagen. Bacterial cells transformed with the plasmids were grown in terrific broth to log phase and treated with 1 mM isopropyl β-D-1-thiogalactopyranoside (IPTG) at 37°C for 3.5 h to induce the expression of recombinant proteins. Expressed recombinant proteins then were purified using nickel-nitrilotriacetic acid (Ni-NTA) agarose resin from Qiagen. Lysis buffer and wash buffer were composed of 20 mM sodium phosphate, 300 mM NaCl, 20 mM imidazole, pH 7.4, and 20 mM sodium phosphate; 300 mM NaCl, 500 mM imidazole, pH 7.4, was used for elution buffer. For cleaving 6His-SUMO (Small Ubiquitin-like Modifier) tags off the purified proteins, recombinant 6His-Ulp1 was used. Cleaved 6His-SUMO tags and 6His-Ulp1 were removed using Ni-NTA resin. Purity of proteins was determined by SDS–PAGE. Proteins were dialyzed into 20 mM sodium phosphate, 150 mM NaCl, 20 mM imidazole, pH 7.4, for pull-down assays or into 50 mM KCl, 2 mM $MgCl_2$, 1 mM ATP, pH 7.5 (F-actin buffer), for actin assembly assays. Concentration of proteins was determined by using Coomassie-stained SDS–PAGE gels with bovine serum albumin standards.

Pull-down assay

Pull-down assays were performed in 20 mM sodium phosphate, 150 mM NaCl, 20 mM imidazole, pH 7.4. Ni-NTA resins was washed with the pull-down buffer first and then incubated with proteins at 4°C overnight. Resins were washed three times with the buffer to remove unbound proteins. Equivalent molar concentrations of proteins were added, except for Tda2, which was added in excess as it was hard to detect due to its low molecular weight.

Actin assembly assay

Rabbit skeletal actin was purified as described by MacLean-Fletcher and Pollard (1980). Purified actin was stored in 2 mM Tris-HCl, 0.2 mM $CaCl_2$, 0.2 mM ATP, 0.5 mM dithiothreitol (DTT), pH 8.0 (monomeric actin (G-actin) buffer), to prevent assembly into filamentous actin (F-actin). F-actin seeds were prepared by adding one-tenth volume of 10xF-actin buffer (500 mM KCl, 10 mM $MgCl_2$, 10 mM ethylene glycol-bis(β-aminoethyl ether)-*N*,*N*,*N*′,*N*′-tetraacetic acid [EGTA], 5 mM DTT, 100 mM Tris-HCl, pH 7.5) to purified rabbit skeletal actin (7 μM), incubating at room temperature for 4 h, diluting to 1 μM, incubating further 4 h, and sonicating the solution to shear assembled F-actin into smaller pieces. They were spun down briefly (17,000 × *g* at 4°C for 30 s) to remove denatured actin and then kept on ice at least for an hour before use to prevent changes in the number of ends during the course of experiments. Purified and clarified actin in G-actin buffer was mixed with pyrene-labeled actin (Cytoskeleton) at 5% and then diluted into 0.056 mg/ml. The actin solution was centrifuged at 100,000 × *g* for 30 min to remove any F-actin that might have formed. After addition of one-tenth volume of 10xCa^{2+}-Mg^{2+} exchange buffer for 2 min, the assembly assay was run at room temperature by mixing 135 μl G-actin, 10 μl protein solutions in 1xF-actin buffer, 15 μl 10xF-actin buffer, and 20 μl F-actin seeds to yield a final concentration of 0.042 mg/ml (1 μM) actin. F-actin seeds were tested at least twice at the beginning and end of experiments to ensure the reproducibility of the seeds. Pyrene fluorescence intensity was measured by a fluorometer (Photon Technology International, PTI) with a setting of 365 nm for excitation and 407 nm for emission. Because this fluorometer does not have an injection system, we opened the housing when adding to the reaction, which gave readings close to 0 during the open period.

Cosedimentation assay

Actin filaments in 1xF-actin buffer were incubated with Aim21/Tda2 in 1xF-actin buffer or equivalent volume of 1xF-actin buffer for 30 min at 4°C. They were then pelleted by centrifugation (160,000 × *g* for 30 min at 4°C). The top 90% of the reaction was taken as supernatant, and the remainder was taken as pellet.

ACKNOWLEDGMENTS

We thank all member of the Bretscher lab for discussion and reading the manuscript. This work was supported by National Institutes of Health grant GM39066.

REFERENCES

Adams AE, Pringle JR (1984). Relationship of actin and tubulin distribution to bud growth in wild-type and morphogenetic-mutant Saccharomyces cerevisiae. J Cell Biol 98, 934–945.

Albuquerque CP, Smolka MB, Payne SH, Bafna V, Eng J, Zhou H (2008). A multidimensional chromatography technology for in-depth phosphoproteome analysis. Mol Cell Proteomics 7, 1389–1396.

Amatruda JF, Cannon JF, Tatchell K, Hug C, Cooper JA (1990). Disruption of the actin cytoskeleton in yeast capping protein mutants. Nature 344, 352–354.

Amatruda JF, Cooper JA (1992). Purification, characterization, and immunofluorescence localization of Saccharomyces cerevisiae capping protein. J Cell Biol 117, 1067–1076.

Amatruda JF, Gattermeir DJ, Karpova TS, Cooper JA (1992). Effects of null mutations and overexpression of capping protein on morphogenesis, actin distribution and polarized secretion in yeast. J Cell Biol 119, 1151–1162.

Burston HE, Maldonado-Baez L, Davey M, Montpetit B, Schluter C, Wendland B, Conibear E (2009). Regulators of yeast endocytosis identified by systematic quantitative analysis. J Cell Biol 185, 1097–1110.

Campellone KG, Welch MD (2010). A nucleator arms race: cellular control of actin assembly. Nat Rev Mol Cell Biol 11, 237–251.

Carlier MF, Laurent V, Santolini J, Melki R, Didry D, Xia GX, Hong Y, Chua NH, Pantaloni D (1997). Actin depolymerizing factor (ADF/cofilin) enhances the rate of filament turnover: implication in actin-based motility. J Cell Biol 136, 1307–1322.

Catlett NL, Weisman LS (1998). The terminal tail region of a yeast myosin-V mediates its attachment to vacuole membranes and sites of polarized growth. Proc Natl Acad Sci USA 95, 14799–14804.

Chernyakov I, Santiago-Tirado F, Bretscher A (2013). Active segregation of yeast mitochondria by Myo2 is essential and mediated by Mmr1 and Ypt11. Curr Biol 23, 1818–1824.

Cope MJ, Yang S, Shang C, Drubin DG (1999). Novel protein kinases Ark1p and Prk1p associate with and regulate the cortical actin cytoskeleton in budding yeast. J Cell Biol 144, 1203–1218.

Drees B, Brown C, Barrell BG, Bretscher A (1995). Tropomyosin is essential in yeast, yet the TPM1 and TPM2 products perform distinct functions. J Cell Biol 128, 383–392.

Evangelista M, Pruyne D, Amberg DC, Boone C, Bretscher A (2002). Formins direct Arp2/3-independent actin filament assembly to polarize cell growth in yeast. Nat Cell Biol 4, 32–41.

Fagarasanu A, Fagarasanu M, Eitzen GA, Aitchison JD, Rachubinski RA (2006). The peroxisomal membrane protein Inp2p is the peroxisome-specific receptor for the myosin V motor Myo2p of Saccharomyces cerevisiae. Dev Cell 10, 587–600.

Farrell KB, McDonald S, Lamb AK, Worcester C, Peersen OB, Di Pietro SM (2017). Novel function of a dynein light chain in actin assembly during clathrin-mediated endocytosis. J Cell Biol 216, 2565–2580.

Fazi B, Cope MJ, Douangamath A, Ferracuti S, Schirwitz K, Zucconi A, Drubin DG, Wilmanns M, Cesareni G, Castagnoli L (2002). Unusual binding properties of the SH3 domain of the yeast actin-binding protein Abp1: structural and functional analysis. J Biol Chem 277, 5290–5298.

Fujiwara T, Tanaka K, Mino A, Kikyo M, Takahashi K, Shimizu K, Takai Y (1998). Rho1p-Bni1p-Spa2p interactions: implication in localization of Bni1p at the bud site and regulation of the actin cytoskeleton in Saccharomyces cerevisiae. Mol Biol Cell 9, 1221–1233.

Gao L, Bretscher A (2008). Analysis of unregulated formin activity reveals how yeast can balance F-actin assembly between different microfilament-based organizations. Mol Biol Cell 19, 1474–1484.

Gavin AC, Aloy P, Grandi P, Krause R, Boesche M, Marzioch M, Rau C, Jensen LJ, Bastuck S, Dumpelfeld B, *et al.* (2006). Proteome survey reveals modularity of the yeast cell machinery. Nature 440, 631–636.

Gietz RD, Schiestl RH (2007). High-efficiency yeast transformation using the LiAc/SS carrier DNA/PEG method. Nat Protoc 2, 31–34.

Goode BL, Eskin JA, Wendland B (2015). Actin and endocytosis in budding yeast. Genetics 199, 315–358.

Hess DC, Myers CL, Huttenhower C, Hibbs MA, Hayes AP, Paw J, Clore JJ, Mendoza RM, Luis BS, Nislow C, *et al.* (2009). Computationally driven, quantitative experiments discover genes required for mitochondrial biogenesis. PLoS Genet 5, e1000407.

Hill KL, Catlett NL, Weisman LS (1996). Actin and myosin function in directed vacuole movement during cell division in Saccharomyces cerevisiae. J Cell Biol 135, 1535–1549.

Hoepfner D, van den Berg M, Philippsen P, Tabak HF, Hettema EH (2001). A role for Vps1p, actin, and the Myo2p motor in peroxisome abundance and inheritance in Saccharomyces cerevisiae. J Cell Biol 155, 979–990.

Johnston GC, Prendergast JA, Singer RA (1991). The Saccharomyces cerevisiae MYO2 gene encodes an essential myosin for vectorial transport of vesicles. J Cell Biol 113, 539–551.

Kaksonen M, Sun Y, Drubin DG (2003). A pathway for association of receptors, adaptors, and actin during endocytic internalization. Cell 115, 475–487.

Kaksonen M, Toret CP, Drubin DG (2005). A modular design for the clathrin- and actin-mediated endocytosis machinery. Cell 123, 305–320.

Kamei T, Tanaka K, Hihara T, Umikawa M, Imamura H, Kikyo M, Ozaki K, Takai Y (1998). Interaction of Bnr1p with a novel Src homology 3 domain-containing Hof1p. Implication in cytokinesis in Saccharomyces cerevisiae. J Biol Chem 273, 28341–28345.

Kim K, Yamashita A, Wear MA, Maeda Y, Cooper JA (2004). Capping protein binding to actin in yeast: biochemical mechanism and physiological relevance. J Cell Biol 164, 567–580.

Kubler E, Riezman H (1993). Actin and fimbrin are required for the internalization step of endocytosis in yeast. EMBO J 12, 2855–2862.

Kulak NA, Pichler G, Paron I, Nagaraj N, Mann M (2014). Minimal, encapsulated proteomic-sample processing applied to copy-number estimation in eukaryotic cells. Nat Methods 11, 319–324.

Lipatova Z, Tokarev AA, Jin Y, Mulholland J, Weisman LS, Segev N (2008). Direct interaction between a myosin V motor and the Rab GTPases Ypt31/32 is required for polarized secretion. Mol Biol Cell 19, 4177–4187.

Liu H, Bretscher A (1992). Characterization of TPM1 disrupted yeast cells indicates an involvement of tropomyosin in directed vesicular transport. J Cell Biol 118, 285–299.

Liu HP, Bretscher A (1989a). Disruption of the single tropomyosin gene in yeast results in the disappearance of actin cables from the cytoskeleton. Cell 57, 233–242.

Liu HP, Bretscher A (1989b). Purification of tropomyosin from Saccharomyces cerevisiae and identification of related proteins in Schizosaccharomyces and Physarum. Proc Natl Acad Sci USA 86, 90–93.

Longtine MS, McKenzie A 3rd, Demarini DJ, Shah NG, Wach A, Brachat A, Philippsen P, Pringle JR (1998). Additional modules for versatile and economical PCR-based gene deletion and modification in Saccharomyces cerevisiae. Yeast 14, 953–961.

MacLean-Fletcher S, Pollard TD (1980). Identification of a factor in conventional muscle actin preparations which inhibits actin filament self-association. Biochem Biophys Res Commun 96, 18–27.

Michelot A, Grassart A, Okreglak V, Costanzo M, Boone C, Drubin DG (2013). Actin filament elongation in Arp2/3-derived networks is controlled by three distinct mechanisms. Dev Cell 24, 182–195.

Moon AL, Janmey PA, Louie KA, Drubin DG (1993). Cofilin is an essential component of the yeast cortical cytoskeleton. J Cell Biol 120, 421–435.

Moseley JB, Goode BL (2005). Differential activities and regulation of Saccharomyces cerevisiae formin proteins Bni1 and Bnr1 by Bud6. J Biol Chem 280, 28023–28033.

Okada K, Ravi H, Smith EM, Goode BL (2006). Aip1 and cofilin promote rapid turnover of yeast actin patches and cables: a coordinated mechanism for severing and capping filaments. Mol Biol Cell 17, 2855–2868.

Ono S, Mohri K, Ono K (2004). Microscopic evidence that actin-interacting protein 1 actively disassembles actin-depolymerizing factor/Cofilin-bound actin filaments. J Biol Chem 279, 14207–14212.

Peng Y, Grassart A, Lu R, Wong CC, Yates J 3rd, Barnes G, Drubin DG (2015). Casein kinase 1 promotes initiation of clathrin-mediated endocytosis. Dev Cell 32, 231–240.

Pringle JR, Preston RA, Adams AE, Stearns T, Drubin DG, Haarer BK, Jones EW (1989). Fluorescence microscopy methods for yeast. Methods Cell Biol 31, 357–435.

Pruyne D, Evangelista M, Yang C, Bi E, Zigmond S, Bretscher A, Boone C (2002). Role of formins in actin assembly: nucleation and barbed-end association. Science 297, 612–615.

Pruyne D, Legesse-Miller A, Gao L, Dong Y, Bretscher A (2004). Mechanisms of polarized growth and organelle segregation in yeast. Annu Rev Cell Dev Biol 20, 559–591.

Pruyne DW, Schott DH, Bretscher A (1998). Tropomyosin-containing actin cables direct the Myo2p-dependent polarized delivery of secretory vesicles in budding yeast. J Cell Biol 143, 1931–1945.
Rodal AA, Manning AL, Goode BL, Drubin DG (2003). Negative regulation of yeast WASp by two SH3 domain-containing proteins. Curr Biol 13, 1000–1008.
Sagot I, Klee SK, Pellman D (2002a). Yeast formins regulate cell polarity by controlling the assembly of actin cables. Nat Cell Biol 4, 42–50.
Sagot I, Rodal AA, Moseley J, Goode BL, Pellman D (2002b). An actin nucleation mechanism mediated by Bni1 and profilin. Nat Cell Biol 4, 626–631.
Schott D, Ho J, Pruyne D, Bretscher A (1999). The COOH-terminal domain of Myo2p, a yeast myosin V, has a direct role in secretory vesicle targeting. J Cell Biol 147, 791–808.
Shortle D, Haber JE, Botstein D (1982). Lethal disruption of the yeast actin gene by integrative DNA transformation. Science 217, 371–373.
Skruzny M, Brach T, Ciuffa R, Rybina S, Wachsmuth M, Kaksonen M (2012). Molecular basis for coupling the plasma membrane to the actin cytoskeleton during clathrin-mediated endocytosis. Proc Natl Acad Sci USA 109, E2533–E2542.
Tonikian R, Xin X, Toret CP, Gfeller D, Landgraf C, Panni S, Paoluzi S, Castagnoli L, Currell B, Seshagiri S, *et al*. (2009). Bayesian modeling of the yeast SH3 domain interactome predicts spatiotemporal dynamics of endocytosis proteins. PLoS Biol 7, e1000218.
van Leeuwen J, Pons C, Mellor JC, Yamaguchi TN, Friesen H, Koschwanez J, Usaj MM, Pechlaner M, Takar M, Usaj M, *et al*. (2016). Exploring genetic suppression interactions on a global scale. Science 354, aag0839.
Weinberg J, Drubin DG (2012). Clathrin-mediated endocytosis in budding yeast. Trends Cell Biol 22, 1–13.
Winder SJ, Jess T, Ayscough KR (2003). SCP1 encodes an actin-bundling protein in yeast. Biochem J 375, 287–295.
Yin H, Pruyne D, Huffaker TC, Bretscher A (2000). Myosin V orientates the mitotic spindle in yeast. Nature 406, 1013–1015.
Yu H, Braun P, Yildirim MA, Lemmens I, Venkatesan K, Sahalie J, Hirozane-Kishikawa T, Gebreab F, Li N, Simonis N, *et al*. (2008). High-quality binary protein interaction map of the yeast interactome network. Science 322, 104–110.